scientific reports

Check for updates

OPEN

Automated synthesis and preliminary evaluation of [^{18}F] FDPA for cardiac inflammation imaging in rats after myocardial infarction

Tiantian Mou[1,3], Jing Tian[1,3], Yi Tian[1], Mingkai Yun[1], Junqi Li[1], Wei Dong[1], Xia Lu[1], Ziwei Zhu[1], Hongzhi Mi[1], Xiaoli Zhang[1]✉ & Xiang Li[1,2]

A translocator protein 18 kDa targeted radiotracer, *N*,*N*-diethyl-2-(2-(4-[^{18}F]fluorophenyl)-5,7-dimethylpyrazolo[1,5-a] pyrimidin-3-yl) acetamide ([^{18}F]FDPA), was automated synthetized and evaluated for cardiac inflammation imaging. Various reaction conditions for an automated synthesis were systematically optimized. MicroPET/CT imaging were performed on normal rats and rats with myocardial infarction (MI). Normalized SUV ratios of [^{18}F]FDPA to [^{13}N]NH_3 (NSRs) in different regions were calculated to normalize the uptake of [^{18}F]FDPA to perfusion. The amount of TBAOMs and the volume/proportion of water were crucial for synthesis. After optimization, the total synthesis time was 68 min. The non-decay corrected radiochemical yields (RCYs) and molar activities were 19.9 ± 1.7% and 169.7 ± 46.5 GBq/μmol, respectively. In normal rats, [^{18}F]FDPA showed a high and stable cardiac uptake and fast clearance from other organs. In MI rats, NSRs in the peri-infarct and infarct regions, which were infiltrated with massive inflammatory cells revealed by pathology, were higher than that in the remote region (1.20 ± 0.01 and 1.08 ± 0.10 vs. 0.89 ± 0.05, respectively). [^{18}F]FDPA was automated synthesized with high RCYs and molar activities. It showed a high uptake in inflammation regions and offered a wide time window for cardiac imaging, indicating it could be a potential cardiac inflammation imaging agent.

Abbreviations

TSPO	Translocator protein 18 kDa
PET	Positron emission tomography
[^{18}F]FDPA	*N*,*N*-Diethyl-2-(2-(4-[^{18}F]fluorophenyl)-5,7-dimethylpyrazolo[1,5-a]pyrimidin-3-yl) acetamide
RCC	Radiochemical conversion
RCY	Radiochemical yield
DPA-SPIAD	2-(2-(4-(((1*r*,3*r*,5*r*,7*r*)-4′,6′-Dioxospiro[adamantane-2,2′-[1,3]dioxan]-5′-ylidene)-λ^3-iodaneyl)phenyl)-5,7-dimethylpyrazolo[1,5-*a*]pyrimidin-3-yl)-*N*,*N*-diethylacetamide
TBAOMs	Tetrabutylammonium methanesulfonate
PK11195	1-(2-Chlorophenyl)-*N*-methyl-*N*-(1-methylpropyl)-3-isoquinolinecarboxamide
SPE	Solid phase extraction
NH_4Ac	Ammonium acetate
t_R	Retention time
RCP	Radiochemical purity
MI	Myocardial infarction
SUV	Standardized uptake value
NSR	Normalized SUV ratio of [^{18}F]FDPA to [^{13}N]NH_3

[1]Department of Nuclear Medicine, Beijing Anzhen Hospital, Capital Medical University, No. 2 Anzhen Road, Chaoyang District, Beijing 100029, China. [2]Division of Nuclear Medicine, Department of Biomedical Imaging and Image-Guided Therapy, Medical University of Vienna, Vienna, Austria. [3]These authors contributed equally: Tiantian Mou and Jing Tian. ✉email: xlzhang68@126.com

No.	Amount of TBAOMs (mg)	H_2O (mL)	CH_3CN (mL)	Elution efficiency (%)
1	12	0.3	0.7	37.6 ± 0.04
2	12	0.3	0.3	79.5 ± 0.03
3	12	0.4	0.6	72.6 ± 0.05
4	12	0.4	0.4	82.3 ± 0.04
5	12	0.4	0.2	85.3 ± 0.01
6	15	0.4	0.4	89.8 ± 0.01
7	20	0.3	0.3	91.9 ± 0.02
8	20	0.4	0.4	98.2 ± 0.01

Table 1. The elution efficiency of [^{18}F]FDPA from the QMA cartridge using different kinds of stock solution (n = 3).

H&E	Hematoxylin and eosin
SD	Standard deviation
ANOVA	Analysis of variance

Translocator protein 18 kDa (TSPO) is mainly localized in the outer mitochondrial membrane. It is associated with various biological processes such as controlling the translocation of cholesterol, regulating mitochondrial membrane potential, mediating immune response, modulating voltage dependent calcium channels and apoptosis[1]. Since it is overexpressed in the activated microglia, the TSPO targeted imaging was focused on evaluating neuroinflammation in the past, including Alzheimer's disease, Parkinson's disease and dementia[2–4].

Mitochondria take up 20–30% of the myocardial intracellular volume[5], making TSPO an attractive biomarker for the diagnosis and evaluation the treatment effects of cardiac diseases[6–8]. Inflammation plays an important role in the healing process after myocardial ischemia[9]. Some clinical trials of anti-inflammatory drugs have been performed on patients with acute myocardial ischemia[10,11]. TSPO is also involved in cardiac inflammation related to macrophage infiltration[12]. Therefore, it might be used to monitor inflammatory response, facilitating physicians to choose the appropriate patients and right time for intervention. Positron emission tomography (PET) is a noninvasive technology to monitor functional and physiological changes in vivo. Currently, several studies reported that TSPO PET imaging could assess cardiac inflammation, such as myocarditis[13,14] and inflammation after ischemia[15], making it a "hot target" for cardiac inflammation imaging.

N,N-Diethyl-2-(2-(4-[^{18}F]fluorophenyl)-5,7-dimethylpyrazolo[1,5-a]pyrimidin-3-yl)acetamide ([^{18}F]FDPA) was reported as a TSPO ligand with an excellent binding affinity (K_i = 2 nM) and a good metabolic stability[16,17]. But the difficulty in fluorine-18 labeling limited its further application. The radiofluorination reaction via [^{18}F] fluoride reported in 2015 resulted in low radiochemical conversions (RCCs, < 3%)[17]. Olof Solin, et al. started with carrier-added [^{18}F]F_2 to prepare [^{18}F]FDPA. The decay corrected radiochemical yields (RCYs) were increased to 15 ± 3%, but the molar activities were still not satisfied (7.8 ± 0.5 GBq/μmol)[18]. In 2017, Lu Wang, et al. used the adamantyl auxiliary-based precursor 2-(2-(4-(((1*r*,3*r*,5*r*,7*r*)-4′,6′-dioxospiro[adamantane-2,2′-[1,3]dioxan]-5′-ylidene)-λ^3-iodaneyl)phenyl)-5,7-dimethylpyrazolo[1,5-*a*]pyrimidin-3-yl)-*N,N*-diethylacetamide (DPA-SPIAD) to manually prepare [^{18}F]FDPA, and dramatically improved both decay corrected RCYs (45 ± 8%) and molar activities (96 ± 22 GBq/μmol)[19], making the further evaluation of [^{18}F]FDPA possible.

In this report, we optimized an automated synthesis of [^{18}F]FDPA based on the previously reported spirocyclic iodonium ylide method[19], and were first to evaluate [^{18}F]FDPA for myocardial inflammation imaging.

Materials and methods

Materials. The precursor DPA-SPIAD and the standard compound [^{19}F]FDPA were purchased from Shenzhen PET-BiO Technology Co., Ltd. (China). Tetrabutylammonium methanesulfonate (TBAOMs), anhydrous CH_3CN, and 1-(2-Chlorophenyl)-*N*-methyl-*N*-(1-methylpropyl)-3-isoquinolinecarboxamide (PK11195) were purchased from Sigma-Aldrich (Germany). O-18 enriched water (purity ≥ 98%) was purchased from Jiangsu Huayi Technology Co., Ltd (China). Other chemicals and reagents were purchased from commercial supplies, without further purification.

Radionuclide production. [^{18}F]fluoride was produced via the ^{18}O (p, n) ^{18}F nuclear reaction by a 11 MeV cyclotron (Eclipse HP, Siemens, USA). A tantalum target containing 2.6 mL O-18 enriched water was irradiated with a proton beam (Target current: 50 μA). At the end of bombardment, [^{18}F]fluoride was delivered into a V-vial in CFN-MPS200 Module (Sumitomo Heavy Industries, Ltd., Tokyo, Japan), and then trapped on a QMA exchange solid phase extraction (SPE) cartridge (Waters Corporation, USA), which was pre-activated by 1 mL of 7.4% $NaHCO_3$ (aq.) and 10 mL of sterile water.

Elution efficiency tests. To improve the elution efficiency of [^{18}F]fluoride, the stock solution containing different amounts of TBAOMs, water and CH_3CN was tested manually (Table 1). For each test, 333–555 MBq [^{18}F]fluoride was trapped on a QMA cartridge, and measured with a dose calibrator (CRC-25R, Capintec. Inc., USA). Then [^{18}F]fluoride was eluted to a vial by different kinds of stock solution, respectively. The radioactivity

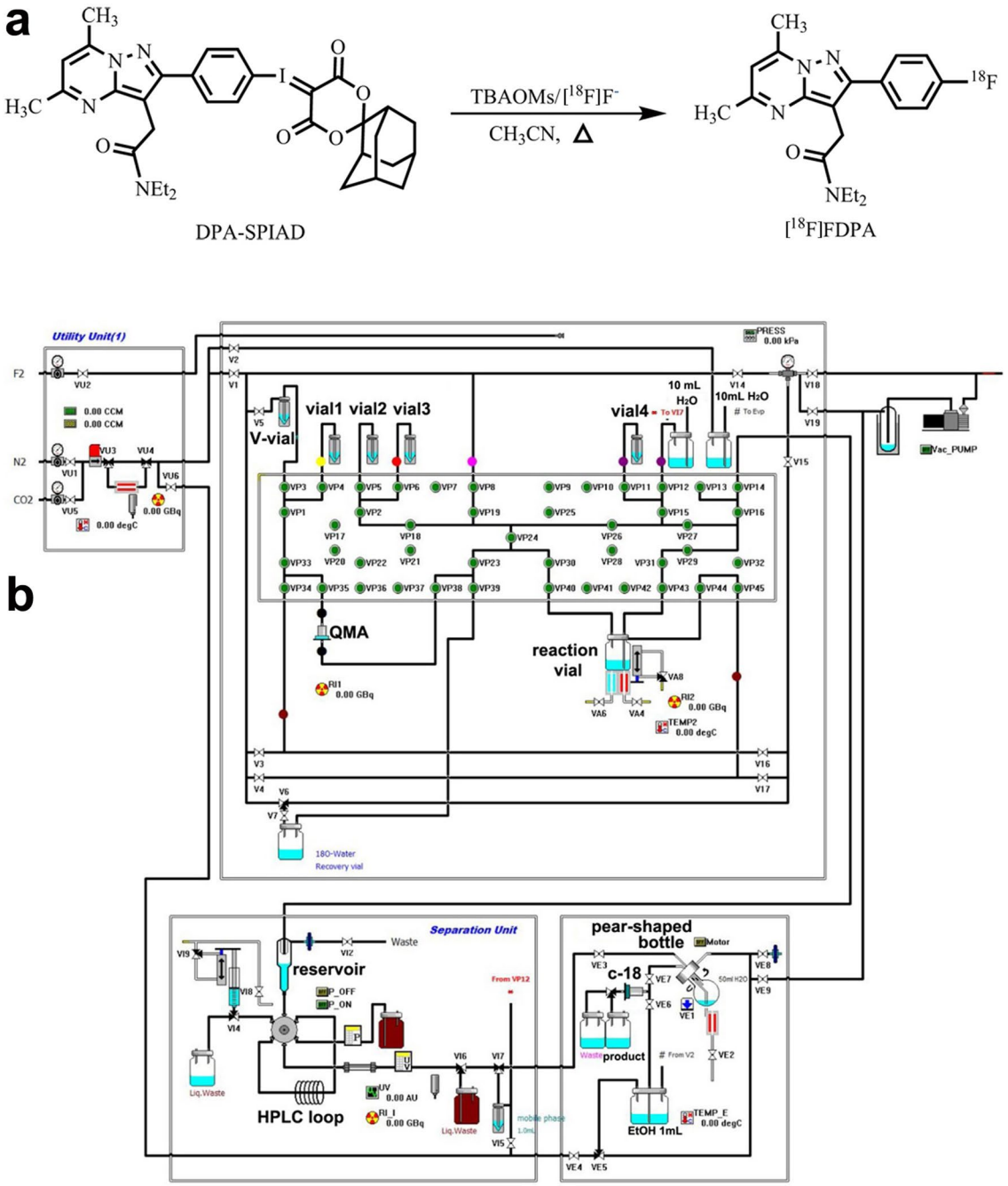

Figure 1. The synthesis route of [^{18}F]FDPA. (**a**) The synthesis route of [^{18}F]FDPA. (**b**) The diagram of the synthesis cassette of CFN-MPS200 module for [^{18}F]FDPA.

of [^{18}F]fluoride solution was measured subsequently. Elution efficiency = (the radioactivity of [^{18}F]fluoride solution / the radioactivity on QMA cartridge) × 100%.

Labeling tests. The labeling method was shown in Fig. 1. To optimize the automated synthesis process of [^{18}F]FDPA, different reaction temperature and reaction time were tested using CFN-MPS200 module. Briefly, 3.7–14.8 GBq [^{18}F]fluoride on a QMA cartridge was eluted to the reaction vial with TBAOMs solution (20 mg TBAOMs in 0.4 mL H_2O and 0.4 mL CH_3CN), and dried under N_2 flow at 100 °C. Anhydrous CH_3CN (0.5 mL) was added, followed by a 4 min evaporation. DPA-SPIAD (2 mg in 1.2 mL CH_3CN) was added into the reaction vial and reaction was evaluated at different temperatures and maintained for different times (Table 2). After each reaction trial was completed, the reaction mixture was analyzed by HPLC (1260II, Agilent Technologies, USA) to calculate the RCC. The analytical HPLC column (SB-C18, 5 μm, 4.6 × 250 mm, Agilent Technologies, USA) was eluted with 50% 0.1 M ammonium acetate (NH_4Ac, solvent A) and 50% CH_3CN (solvent B) at a flow rate of 1 mL/min. The radio-peak for [^{18}F]FDPA was confirmed with the corresponding retention time (t_R) determined

#	Reaction temperature (°C)	Reaction time (min)	RCC (%)
1	90	15	4.2
2	100	10	62.7
3	100	15	74.6
4	100	20	50.8
5	120	10	57.4
6	120	15	64.2
7	120	20	40.4

Table 2. The RCC of [^{18}F]FDPA in different reaction conditions.

from the standard compound [^{19}F]FDPA. RCC = (the area of radio-peak of [^{18}F]FDPA/the summed areas of all radio-peaks) × 100%.

Adsorption rate of sterile filters. Three kinds of sterile filters, Mtllex-GS (Merck Millipore, Germany), Minisart (Sartorius Stedim Biotech, Germany) and Cathivex-GV (Merck Millipore, Germany) were tested manually. 740–1110 MBq of [^{18}F]FDPA in 10% ethanol solution was passed through different filters and collected with a vial, respectively. The radioactivity of filters and [^{18}F]FDPA solution in vials was measured soon afterwards. The adsorption rate = (the radioactivity of the filter/the summed radioactivities of the filter and [^{18}F]FDPA solution) × 100%.

Final automated synthesis process. The optimal synthesis process was described as follows (Fig. 1). At the beginning of automated synthesis, [^{18}F]fluoride (33.3–40.7 GBq) was trapped on a QMA cartridge, and eluted to the reaction vial with TBAOMs solution (20 mg TBAOMs in 0.4 mL H_2O and 0.4 mL CH_3CN) from Vial 1. The solvent was removed by reduced pressure distillation under N_2 flow at 100 °C for 7 min. Anhydrous CH_3CN (0.5 mL) from Vial 2 was added to the reaction vial and heated at 95 °C under N_2 flow for 4 min. DPA-SPIAD (2 mg in 1.2 mL CH_3CN) from Vial 3 was added into the reaction vial. Then, the reaction vial was sealed and heated at 100 °C for 15 min. Subsequently, the reaction mixture was cooled to 30 °C and diluted with 1 mL water from Vial 4. The crude reaction mixture was transferred to the reservoir, and then injected onto the HPLC loop with a 2.5 mL syringe. After the automated injection, the semi-preparative column (YMC-Pack ODS-AM C18 semi-preparative column, 250 × 10 mm, 5 μm, YMC Co., Ltd., Japan) was eluted with 50:50 CH_3CN/0.1 M NH_4Ac by volume at a flow rate of 4 mL/min. According to ultraviolet (UV, λ = 254 nm) and radiochemical detectors of the module, the desired product (t_R = 16.5–17.5 min) was collected into a pear-shaped bottle preloaded with 50 mL water. The mixture was trapped on a C18 SPE cartridge (Waters Corporation, USA), and washed with 10 mL water. The product was eluted with 1 mL ethanol to product vial subsequently, followed by 10 mL sterile water. The solution was passed through a Cathivex-GV filter, and collected with a 25 mL sterile vial.

The radiochemical purity (RCP) and molar activity of the final [^{18}F]FDPA solution were determined by re-injecting the product onto the analytical HPLC column and analyzed with the HPLC method mentioned above. The radioactive fraction was measured by a radio detector (Flow-Count, Bioscan Inc., USA) for molar activity calculation. The mass of the product was calculated by comparing the area under the UV curve at 254 nm with that of standard reference.

Animal model. Male Sprague–Dawley rats (300–350 g) were purchased from SPF (Beijing) Biotechnology Co., Ltd. (China). Rats were maintained in a temperature-controlled room (25 °C) with a natural day/night cycle and fed with a standard rodent diet and water.

For myocardial infarction (MI) modeling, four rats were anesthetized with an air flow containing 4.0% isoflurane. A left thoracotomy was performed between the third and fourth ribs of the rat. The left pericardium was opened. The left anterior descending branch (LAD) was permanently ligated 1–2 mm below the left atrial appendage, using a 7-0 polypropylene suture with a small curved needle. Successful coronary occlusion was verified by observing the myocardium turned grey after LAD ligation.

All animal experiments were performed according to the laboratory animal management regulations of Beijing, and approved by the Animal Care Committee of Capital Medical University.

MicroPET/CT imaging protocol. PET/CT imaging studies were performed with a dedicated microPET/CT scanner (Inveon PET/CT, Siemens, Germany). The imaging protocols were shown in Fig. 2.

On the 6th day after surgery, MI rats (350–400 g, n = 3) and normal rats (350–400 g, n = 3) were performed [^{18}F]FDPA imaging study. The rat was placed into a chamber connected to an isoflurane anesthesia unit. Anesthesia was induced using an air flow rate of 2.0 L/min containing 4.0% isoflurane. Then, the animal was immediately placed in a prone position on the scanning bed. The air flow rate was then reduced to 0.8–1.5 L/min with 1–1.5% isoflurane.[^{18}F]FDPA (25–37 MBq) was injected via the tail vein. A 60 min dynamic PET scan (6 frames: 6 × 600 s) was started immediately at the beginning of injection, followed by 10 min CT scan using 'magnification low' acquisition settings (projection: 180; binning: 4 × 4; transaxial field of view: 53.9 mm; axial scanning length: 134 mm; voltage: 80 kV; current: 500 μA). For the blocking study, a MI rat was injected with

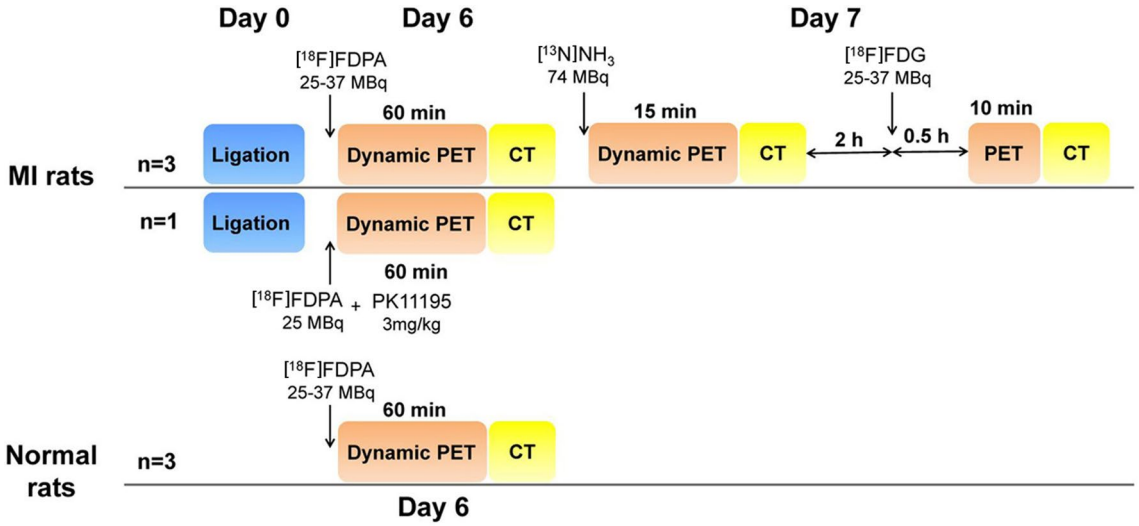

Figure 2. The imaging protocol of microPET/CT with [^{18}F]FDPA, [^{13}N]NH_3 and [^{18}F]FDG, respectively.

a well-known TSPO-selective ligand PK11195 (3 mg/kg) and 25 MBq of [^{18}F]FDPA successively. The imaging protocol was same as above.

On the 7th Day after surgery, the MI rats ($n = 3$) were performed [^{13}N]NH_3 imaging study. About 74 MBq [^{13}N]NH_3 was injected via the tail vein. The PET/CT imaging protocol was similar with that of [^{18}F]FDPA, except the PET scan lasted for 15 min (2 frames: 1×300 s, 1×600 s).

Two hours after [^{13}N]NH_3 imaging, the MI rats ($n = 3$) were anesthetized again for [^{18}F]FDG imaging. [^{18}F]FDG (25–37 MBq) was injected via the tail vein. The PET/CT imaging protocol was similar as that of [^{18}F]FDPA, except the PET scan began at 30 min post-injection (p.i.) and lasted for 10 min (1 frame: 1×600 s).

Image reconstruction. The list-mode data of [^{18}F]FDPA in normal rats were re-histogrammed to 30 frames of 6×20 s, 18×60 s, 4×300 s, 2×600 s for drawing time-activity curves (TACs).

Reconstruction of PET data was performed using a OSEM3D/SP-MAP algorithm (OESM3D: 2 iterations; SP-MAP: 18 iterations; Matrix size: 128×128; Image zoom: 1). CT data were reconstructed using a Feldkamp algorithm (Inveon Research Workplace, Siemens, Germany). PET and CT data were co-registered automatically. A 3D-Guassian filter (1.0 mm FWHM) was applied to smooth noise. The reconstructed images were visualized as coronal, sagittal and transversal slices. Regions of organs were carefully drawn according to the CT images. To draw the different regions of the heart, the data of [^{18}F]FDPA, [^{13}N]NH_3 and [^{18}F]FDG were co-registered by Inveon Research Workplace manually. The infarct region was drawn in the region exhibiting severe defect in both of [^{13}N]NH_3 and [^{18}F]FDG images. The peri-infarct region was drawn in the border of infarcted anterior wall where still revealed [^{18}F]FDG activity. Mean standardized uptake values (SUVs) were calculated by the software automatically. To normalize the uptake of [^{18}F]FDPA to perfusion, the normalized SUV ratio of [^{18}F]FDPA to [^{13}N]NH_3 (NSR) was calculated according to the reported procedure with some modification[20]. NSR = (the mean SUV of [^{18}F]FDPA in region of interest/the max SUV of [^{18}F]FDPA in the heart)/(the mean SUV of [^{13}N]NH_3 in region of interest/the max SUV of [^{13}N]NH_3 in the heart).

Histology. When imaging studies on the 7th Day after surgery were completed, the rats were sacrificed. The hearts were harvested, and fixed with formalin solution. Each sample was embedded in paraffin, cut into serial sections and mounted on glass slides. Sections were stained with hematoxylin and eosin (H&E)[13]. Tissue sections were examined with a light microscope (Leica DM 3000, Leica, Germany) and processed using Leica Application Suite V4.2 microscope software platform.

Statistical analysis. IBM SPSS 19.0 was used for statistical analysis. The data was expressed as mean ± standard deviation (SD). SUVs in the heart at different time points were compared using one-way analysis of variance (ANOVA). NSRs in the peri-infarct, infarct and remote regions at 35 min p.i. were analyzed using Kruskal–Wallis H test. A P value < 0.05 was considered significant.

Results

Optimization of final automated radiosynthesis. As shown in Table 1, when the proportion of water decreased, the elution efficiency decreased remarkably (No.1 vs. No.2, No.3 vs. No.5). Similarly, the stock solution with more volume of water resulted in higher elution efficiency (No.2 vs. No.4, No.7 vs. No.8). On the other hand, more amounts of TBAOMs could improve the elution efficiency as well (No.4 vs. No.6 & No.8). According to Table 1, the best formulation of stock solution was 20 mg TBAOMs in 0.4 mL H_2O and 0.4 mL CH_3CN.

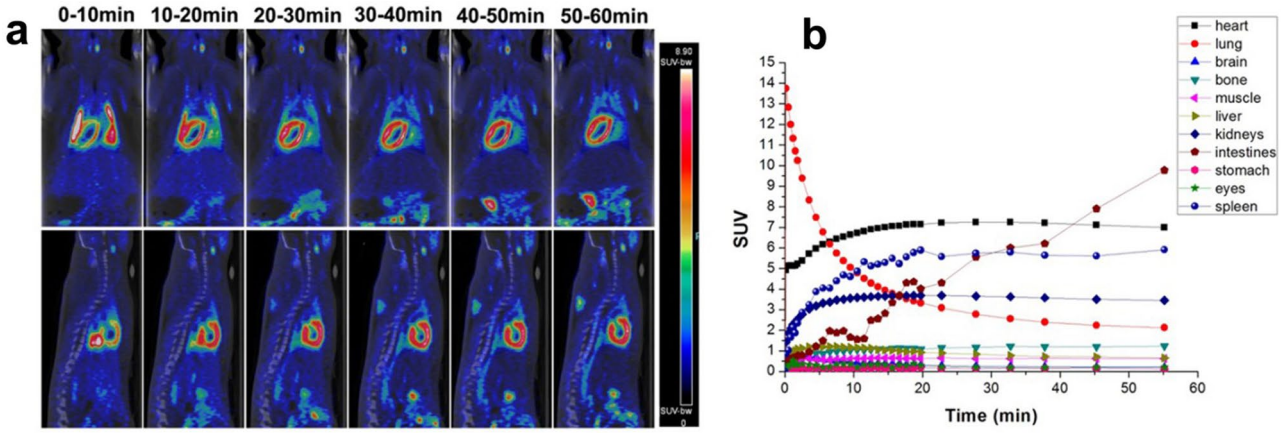

Figure 3. MicroPET/CT imaging studies of [^{18}F]FDPA in normal rats. (**a**) Coronal and sagittal PET/CT images from a normal rat at different timepoints p.i. of [^{18}F]FDPA. (**b**) Time-activity curves of [^{18}F]FDPA obtained from organs of normal rats at 0–60 min p.i., n = 3.

Both reaction temperature and time affected RCC (Table 2). The best condition for labeling was heating at 100 °C for 15 min. When the temperature increased to 120 °C, or the reaction time extended to 20 min, RCC reduced dramatically.

[^{18}F]FDPA could be adsorbed by some sterile filters, leading to low RCYs. In this study, the adsorption rates of Mtllex-GS, Minisart and Cathivex-GV were 96.3 ± 0.02%, 25.4 ± 0.01% and 3.4 ± 0.01%, respectively (n = 3). Cathivex-GV sterile filter was suitable for [^{18}F]FDPA.

Optimal automated synthesis process. The optimal synthesis process was described above. Starting from [^{18}F]fluoride trapped on a QMA cartridge, the total synthesis time was 68 min, including HPLC purification and formulation. The RCYs were 19.9 ± 1.7% (n = 3) without correction. The radio-HPLC retention time of [^{18}F]FDPA (t_R = 13.3 min) was consistent with the corresponding nonradioactive reference (t_R = 12.7 min) (Supplementary Fig. 1). The RCPs ≥ 99%. The molar activities were 169.7 ± 46.5 GBq/μmol (4.6 ± 1.2 Ci/μmol) at the end of synthesis.

MicroPET/CT imaging. In normal rats, TACs indicated that [^{18}F]FDPA mainly accumulated in the heart, lungs, spleen, kidneys and intestines, in which TSPO were highly expressed (Fig. 3). The initial uptake in lungs were too high that the observation of the heart was interfered. Fortunately, the clearance of [^{18}F]FDPA from lungs was fast. At 20–55 min p.i., the heart showed stable and prominent uptake of [^{18}F]FDPA. The SUVs in the heart were 7.15 ± 0.66 at 20 min and 6.99 ± 0.49 at 55 min p.i. respectively, higher than other organs nearby (Fig. 3). Other tissues in which TSPO were barely expressed, such as muscle (SUVs were 0.63 ± 0.11 at 20 min and 0.62 ± 0.01 at 55 min p.i., respectively), exhibited low uptake of [^{18}F]FDPA.

In the [^{13}N]NH_3 images of MI rats (Fig. 4), a severe perfusion defect with significantly reduced [^{13}N]NH_3 activity was observed in the apex and anterior wall. In [^{18}F]FDG images, the extent of reduced [^{18}F]FDG uptake was smaller than that in [^{13}N]NH_3 images. As shown in Fig. 5, [^{18}F]FDPA was accumulated obviously in peri-infarct region, compared with that in remote region or infarct region at 5–55 min p.i. From 25–55 min p.i., the SUVs in peri-infarct regions were maintained consistently, without significant difference (F = 0.064, P = 0.977), as well as the SUVs in remote regions (F = 0.184, P = 0.904) or infarct regions (F = 0.220, P = 0.880) (Fig. 5). At 35 min p.i., the NSRs in the peri-infarct, infarct and remote regions were 1.20 ± 0.01, 1.08 ± 0.10 and 0.89 ± 0.05, respectively (P = 0.027). The NSRs in the peri-infarct, infarct regions were higher than that in remote regions (P = 0.022 and 0.539, respectively). In the blocking study, the uptake of [^{18}F]FDPA was obviously inhibited by PK11195 (Supplementary Fig. 2), which confirmed the affinity of [^{18}F]FDPA to TSPO.

Histology. As shown in Fig. 6, abundant dark purple stains accumulated in the infarct and peri-infarct regions, indicating these regions were infiltrated by inflammatory cells. In contrast, there was few dark purple stains in the remote myocardium.

Discussion

Final automated radiosynthesis. [^{18}F]FDPA is an analog of a well-known TSPO ligand ^{18}F-DPA-714[21,22]. The aryl-^{18}F bond of [^{18}F]FDPA successfully improved the metabolic stability[18,23], but also brought a challenge for fluorine-18 labeling. Compared with the manual method[19], the current study optimized a series of parameters and developed an automated synthesis of [^{18}F]FDPA with better RCC (74.6% vs. 63%), higher molar activities (169.7 ± 46.5 vs. 96 ± 22 GBq/μmol), shorter synthesis time (68 min vs 80 min) and comparable RCYs and RCPs[19]. Compared with the automated method reported recently[24], the process resulted in better RCYs (19.9 ± 1.7% vs. 15.6 ± 4.2%).

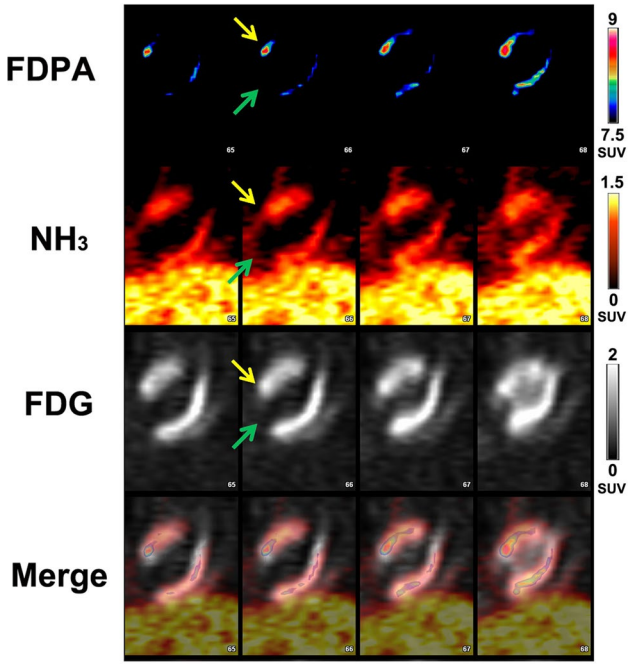

Figure 4. Coronal PET images of a MI rat using [^{18}F]FDPA, [^{18}F]FDG and [^{13}N]NH_3. The pre-infarct region in the anterior wall (yellow arrows) exhibited a localized elevated [^{18}F]FDPA activity, a high [^{18}F]FDG activity and a reduced [^{13}N]NH_3 activity. The infarct region in apex (green arrows) showed severe reduced radioactivity in all images.

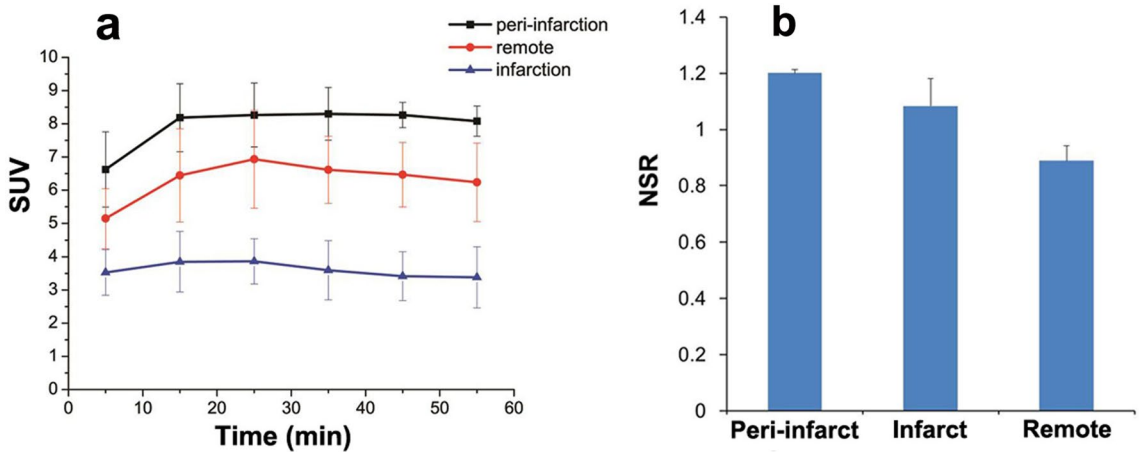

Figure 5. The analysis of radio-uptake in the heart at 0–60 min p.i. (**a**) The SUVs of [^{18}F]FDPA in the peri-infarct, infarct and remote regions at 0–60 min p.i.. SUVs were expressed as mean ± SD (n = 3). (**b**) The normalized SUV ratios of [^{18}F]FDPA to [^{13}N]NH_3 (NSRs) in the peri-infarct, infarct and remote regions at 35 min p.i. (n = 3).

In this study, several key points affected the final radiochemical yield from the automated synthesis using this method. Firstly, the amount of TBAOMs and the volume/proportion of water for [^{18}F]fluoride elution was crucial to achieving higher RCC and molar activity. Though both the increase of volume or proportion of water can rise elution efficiency, the incremental water may also affect the drying efficiency in the next step. Therefore, we optimized the formulation of stock solution as 20 mg TBAOMs in 0.4 mL CH_3CN and 0.4 mL H_2O, instead of the previous method (12 mg TBAOMs in 0.5 mL CH_3CN and 0.5 mL H_2O), and resulted in a satisfied elution efficiency. This formulation of stock solution could be a reference for other automated fluorine-18 labeling with TBAOMs. Secondly, the reaction temperature and time also affected the RCC as reported before[19]. In CFN-MPS200 module, the best reaction temperature and time was 100 °C for 15 min. If the reaction time was prolonged or the temperature was increased, RCC decreased accordingly. This may due to the complete evaporation of CH_3CN under those harsher conditions, which could be observed from the camera of CFN-MPS200 module, leading to no liquid medium available for the reaction. Thirdly, some sterile filters can adversely affect

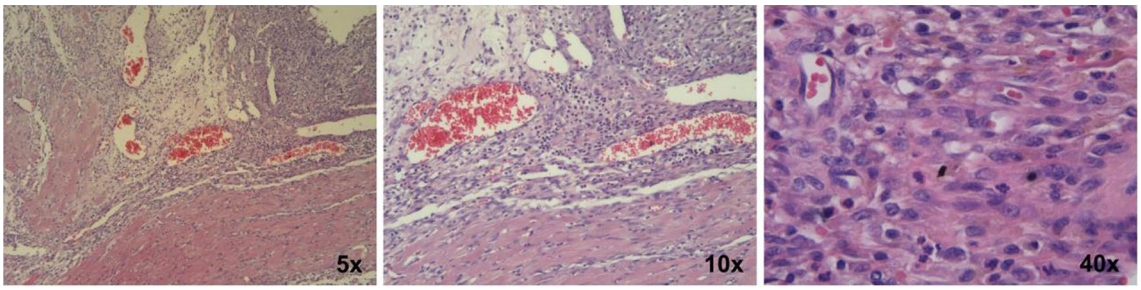

Figure 6. Inflammatory response in the heart of a rat on the 7th day after ligation. Representative H&E histology sections show the infarct and peri-infarct region were infiltrated by inflammatory cells (dark purple stains). The amplification was 5, 10 and 40, respectively.

the final radiochemical yield by adsorbing [^{18}F]FDPA onto the specific filter membranes preventing the quantitative transfer of radioactivity into the final sterile vial.

Cardiac inflammation imaging. In the respective PET imaging studies, the absence of radioactivity uptake in the affected MI regions of both [^{13}N]NH_3 and [^{18}F]FDG images indicated the MI models were successfully made. Low uptake of [^{18}F]FDPA in the liver and the fast clearance from lungs resulted in an improved quality image indicating specific cardiac inflammation when compared to other cardiac inflammation imaging tracers, such as [^{125}I]IodoDPA-713[13], ^{18}F-CB251[14], and ^{68}Ga-NOTA-MSA[25]. The stable uptake of [^{18}F]FDPA in the peri-infarct, infarct and remote regions offered a wider time window for cardiac imaging. The higher NSRs in the peri-infarct and infarct regions compared with that in the remote regions, combined with the result of H&E staining indicated that [^{18}F]FDPA can be accumulated in the inflammation lesions of the heart in MI model.

[^{18}F]FDG is used in clinic for cardiac inflammation imaging. However, the high uptake of [^{18}F]FDG by cardiomyocytes seriously interfere with inflammation imaging. Dietary strategies or unfractionated heparin administration is required for the suppression of the uptake by viable or normal myocytes[26]. A similar phenomenon is observed in this study. Since TSPO was highly expressed in normal cardiomyocytes[12], [^{18}F]FDPA showed certain uptake in normal myocardium, which might complicate the results of cardiac inflammation imaging. Besides that, in the infarct region, due to the dysfunction of mitochondria in cardiomyocyte[15], the SUVs of [^{18}F]FDPA were not as high as that in remote regions, which affected the visual analysis of inflammation. Therefore, the images of TSPO targeted tracers need an appropriate normalization method for cardiac inflammation imaging. Frank M. Bengel et al. used the polar map of ^{99m}Tc-sestamibi as a reference, successfully assessed the elevated signal of a TSPO tracer ^{18}F-GE180 in the infarct region of mice at 1 week post MI[15]. In this study, we used the activity of [^{13}N]NH_3 as a reference, calculated the NSRs in the peri-infarct, infarct and remote regions.

TSPO is associated with various cardiac diseases, such as arrhythmia[27], large vessel vasculitis[28], cardiac hypertrophy[29], atherosclerosis[30] and myocarditis[14]. It is worth mentioning that, TSPO is not only a diagnostic marker, but also a therapeutic target for cardiovascular diseases[12]. TSPO ligands have been studied as therapeutic drugs for cardiovascular diseases, including arrhythmia[27] and MI[31]. Therefore, the quantitative determination of TSPO level by TSPO targeted tracers may offer more valuable information for individual treatment strategy and curative effects. Besides that, since TSPO targeted tracers are prominent for neuroinflammatory imaging, whole-body TSPO imaging may be used to evaluate the systemic inflammatory response in certain diseases. TSPO targeted tracers are worth further investigations. At the meantime, follow-up studies, especially with suitable methods for analysis, are warranted in the future.

Conclusion

The synthesis of [^{18}F]FDPA was successfully optimized and automated with good RCYs, high molar activities, and short synthesis time. The fast clearance of [^{18}F]FDPA from non-target organs and the stable uptake in the heart offered a wider time window for cardiac imaging. Higher NSRs from PET imaging and H&E staining showing the presence of inflammatory cells in the peri-infarct and infarct regions suggest that [^{18}F]FDPA could be a potential imaging agent for cardiac inflammation.

Received: 19 March 2020; Accepted: 19 October 2020
Published online: 29 October 2020

References

1. Surinkaew, S., Chattipakorn, S. & Chattipakorn, N. Roles of mitochondrial benzodiazepine receptor in the heart. *Can. J. Cardiol.* **27**, 262.e3-262.e13 (2011).
2. Alam, M. M., Lee, J. & Lee, S. Y. Recent progress in the development of TSPO PET ligands for neuroinflammation imaging in neurological diseases. *Nucl. Med. Mol. Imaging* **51**, 283–296 (2017).
3. Dupont, A. C. *et al.* Translocator protein-18 kDa (TSPO) positron emission tomography (PET) imaging and its clinical impact in neurodegenerative diseases. *Int. J. Mol. Sci.* **18**, e785 (2017).
4. Brackhan, M. *et al.* [^{18}F]GE180 positron emission tomographic imaging indicates a potential double-hit insult in the intrahippocampal kainate mouse model of temporal lobe epilepsy. *Epilepsia* **59**, 617–626 (2018).

5. Mou, T. & Zhang, X. Research progress on ^{18}F-labeled agents for imaging of myocardial perfusion with positron emission tomography. *Molecules* **22**, e562 (2017).
6. Wang, X., Guo, Z., Ding, Z. & Mehta, J. L. Inflammation, autophagy, and apoptosis after myocardial infarction. *J. Am. Heart Assoc.* **7**, e008024 (2018).
7. Lameijer, M. A., Tang, J., Nahrendorf, M., Beelen, R. H. J. & Mulder, W. J. M. Monocytes and macrophages as nanomedicinal targets for improved diagnosis and treatment of disease. *Expert Rev. Mol. Diagn.* **13**, 567–580 (2013).
8. Largeau, B., Dupont, A. C., Guilloteau, D., Santiago-Ribeiro, M. J. & Arlicot, N. TSPO PET imaging: From microglial activation to peripheral sterile inflammatory diseases?. *Contrast Med. Mol. I.* **2017**, e6592139 (2017).
9. Thackeray, J. T. & Bengel, F. M. Translational molecular nuclear cardiology. *Cardiol. Clin.* **34**, 187–198 (2016).
10. Ridker, P. M. & Luscher, T. F. Anti-inflammatory therapies for cardiovascular disease. *Eur. Heart J.* **35**, 1782–1791 (2014).
11. Shirazi, L. F., Bissett, J., Romeo, F. & Mehta, J. L. Role of inflammation in heart failure. *Curr. Atheroscler. Rep.* **19**, e27 (2017).
12. Qi, X., Xu, J., Wang, F. & Xiao, J. Translocator protein (18 kDa): A promising therapeutic target and diagnostic tool for cardiovascular diseases. *Oxid. Med. Cell Longev.* **2012**, e162934 (2012).
13. Fairweather, D. L. *et al.* Sex differences in translocator protein 18 kDa (TSPO) in the heart: Implications for imaging myocardial inflammation. *J. Cardiovasc. Transl.* **7**, 192–202 (2014).
14. Kim, G. R. *et al.* Assessment of TSPO in a rat experimental autoimmune myocarditis model: A comparison study between [^{18}F] Fluoromethyl-PBR28 and [^{18}F]CB251. *Int. J. Mol. Sci.* **19**, e276 (2018).
15. Thackeray, J. T. & Bengel, F. M. Molecular imaging of myocardial inflammation with positron emission tomography post-ischemia: A determinant of subsequent remodeling or recovery. *JACC Cardiovasc. Imaging* **11**, 1340–1355 (2018).
16. Selleri, S. *et al.* 2-Arylpyrazolo[1,5-a]pyrimidin-3-yl acetamides. New potent and selective peripheral benzodiazepine receptor ligands. *Bioorgan. Med. Chem.* **9**, 2661–2671 (2001).
17. Annelaure, D. *et al.* The pyrazolo[1,5-a]pyrimidine F-DPA: Synthesis, in vitro characterization and radiolabeling with fluorine-18 using a nucleophilic approach. *J. Labelled. Compd. Radiopharm.* **58**, s180 (2015).
18. Keller, T. *et al.* Radiosynthesis and preclinical evaluation of [^{18}F]F-DPA, a novel pyrazolo[1,5a]pyrimidine acetamide TSPO radioligand, in healthy Sprague Dawley rats. *Mol. Imaging. Biol.* **19**, 736–745 (2017).
19. Wang, L. *et al.* A facile radiolabeling of [^{18}F]FDPA via spirocyclic iodonium ylides: Preliminary PET imaging studies in preclinical models of neuroinflammation. *J. Med. Chem.* **60**, 5222–5227 (2017).
20. Thackeray, J. T. *et al.* Myocardial inflammation predicts remodeling and neuroinflammation after myocardial infarction. *J. Am. Coll. Cardiol.* **71**, 263–275 (2018).
21. Miyajima, N. *et al.* Detection of neuroinflammation before selective neuronal loss appearance after mild focal ischemia using [^{18}F] DPA-714 imaging. *EJNMMI. Res.* **8**, e43 (2018).
22. Zinnhardt, B. *et al.* Combined PET imaging of the inflammatory tumor microenvironment identifies margins of unique radiotracer uptake. *Cancer Res.* **77**, 1831–1841 (2017).
23. Keller, T. *et al.* [^{18}F]FDPA for the detection of activated microglia in a mouse model of Alzheimer's disease. *Nucl. Med. Biol.* **67**, 1–9 (2018).
24. Wang, L. *et al.* A concisely automated synthesis of TSPO radiotracer [^{18}F]FDPA based on spirocyclic iodonium ylide (SCIDY) method and validation for human use. *J. Labelled. Compd. Radiopharm.* https://doi.org/10.1002/jlcr.3824 (2020).
25. Seung-Pyo, L. *et al.* Noninvasive imaging of myocardial inflammation in myocarditis using ^{68}Ga-tagged mannosylated human serum albumin positron emission tomography. *Theranostics* **7**, 413–424 (2017).
26. Thackeray, J. T. *et al.* Clinically relevant strategies for lowering cardiomyocyte glucose uptake for ^{18}F-FDG imaging of myocardial inflammation in mice. *Eur. Nucl. Med. Mol. Imaging* **42**, 771–780 (2015).
27. Li, J. *et al.* Inhibition of mitochondrial translocator protein prevents atrial fibrillation. *Eur. J. Pharmacol.* **632**, 60–64 (2010).
28. Pugliese, F. *et al.* Imaging of vascular inflammation with [^{11}C]-PK11195 and positron emission tomography/computed tomography angiography. *J. Am. Coll. Cardiol.* **56**, 653–661 (2010).
29. Maulik, S. K. & Kumar, S. Oxidative stress and cardiac hypertrophy: A review. *Toxicol Mech. Method* **22**, 359–366 (2012).
30. Hellberg, S. *et al.* 18-kDa translocator protein ligand ^{18}F-FEMPA: Biodistribution and uptake into atherosclerotic plaques in mice. *J. Nucl. Cardiol.* **24**, 862–871 (2017).
31. Xiao, J. *et al.* 4'-chlorodiazepam, a translocator protein (18 kDa) antagonist, improves cardiac functional recovery during postischemia reperfusion in rats. *Exp. Biol. Med.* **235**, 478–486 (2010).

Acknowledgements

This work was supported by the Beijing Hospitals Authority Youth Programme (Grant number 20190606), the National Natural Science Foundation of China (Grant numbers 81871377, 81301251, 81571717, 81071177), and Capital Characteristic Clinical Application Research (Grant number Z181100001718071).

Author contributions

X.Z. and T.M. designed the study and wrote the manuscript. T.M. Mou T. carried out synthetic radiochemistry. J.T., Y.T. and J.L. performed the animal experiments. M.Y., W.D., X.L. and Z.Z. analyzed the imaging data. X.Z., H.M. and X.L. reviewed the manuscript.

Competing interests

The authors declare no competing interests.

Additional information

Supplementary information is available for this paper at https://doi.org/10.1038/s41598-020-75705-2.

Correspondence and requests for materials should be addressed to X.Z.

Reprints and permissions information is available at www.nature.com/reprints.

Publisher's note Springer Nature remains neutral with regard to jurisdictional claims in published maps and institutional affiliations.